Talanta 114 (2013) 124–130

Contents lists available at ScienceDirect

Talanta

journal homepage: www.elsevier.com/locate/talanta

Highly sensitive and selective cartap nanosensor based on luminescence resonance energy transfer between $NaYF_4$:Yb,Ho nanocrystals and gold nanoparticles

Zhijiang Wang [a,*,1], Lina Wu [b,1], Baozhong Shen [b], Zhaohua Jiang [a,c,**]

[a] School of Chemical Engineering and Technology, Harbin Institute of Technology, Harbin 150001, China
[b] Key Laboratory of Molecular Imaging in College of Heilongjiang Province, Department of Radiology, The 4th Affiliated Hospital, Harbin Medical University, Harbin 150001, China
[c] State Key Laboratory of Urban Water Resource and Environment, Harbin Institute of Technology, Harbin 150001, China

ARTICLE INFO

Article history:
Received 19 November 2012
Received in revised form
23 February 2013
Accepted 27 February 2013
Available online 7 March 2013

Keywords:
Nanosensor
Cartap
Upconversion nanocrystal
Gold
Luminescence resonance energy transfer

ABSTRACT

Fluorescent detection is an attractive method for the detection of toxic chemicals. However, most chemosensors that are currently utilized in fluorescent detection are based on organic dyes or quantum dots, which suffer from instability, high background noise and interference from organic impurities in solution, which can also be excited by UV radiation. In the present research, we developed a novel $NaYF_4$:Yb,Ho/Au nanocomposite-based chemosensor with high sensitivity (10 ppb) and selectivity over competing analytes for the detection of the insecticide cartap. This nanosensor is excited with a 970-nm laser instead of UV radiation to give an emission peak at 541 nm. In the presence of cartap, the nanocomposites aggregate, resulting in enhanced luminescence resonance energy transfer between the $NaYF_4$:Yb,Ho nanocrystals and the gold nanoparticles, which decreases the emission intensity at 541 nm. The relative luminescence intensity at 541 nm has a linear relationship with the concentration of cartap in the solution. Based on this behavior, the developed nanosensor successfully detected cartap in farm produce and water samples with satisfactory results.

1. Introduction

Environmental pollution by organic toxic chemicals continues to be one of the world's leading challenges to sustainable development. Cartap, which is a nereistoxin derivative, is one of the most widely utilized pesticides in agriculture for crop protection and garden markets [1,2]. The presence of cartap residues in fruit and vegetable crops as well as in water has been shown to inhibit lysyl oxidase activity and cause significant neuromuscular toxicity, resulting in respiratory failure [3,4], and it may also induce multisystem organ failure, thereby leading to human death [5]. Concerns about the toxicological impact of cartap have motivated the exploration of a method to detect and monitor cartap residues. Because of the low concentrations of pesticide and the coexistence of matrix interferences, a detection method that is rapid, sensitive and selective for the target molecule in food and environmental matrices is highly desired. A number of technologies, including gas chromatography–mass spectrometry (GC–MS) [6] and liquid chromatography–mass spectrometry (LC–MS) [7], have been utilized to detect cartap. In spite of their enhanced specificity and sensitivity, these GC/LC-MS-based methods have the disadvantages of utilizing expensive equipment, being time-consuming and being complicated.

Fluorescence detection with pesticide-responsive chemosensors offers a promising approach for the simple and rapid tracking of these deleterious compounds [8–10]. In particular, luminescence resonance energy transfer (LRET) technology is convenient and can be applied routinely at the single molecule detection limit, making it an ideal method to detect trace amount of pesticides [11–15]. Unfortunately, most of these nanosensors are based on organic fluorophores or quantum dots, which are excited by UV or visible radiation. In the application of these detection techniques, the many impurities that are present in biological, toxicological and environmental samples can also be excited under such conditions, thereby reducing the detection sensitivity.

Identifying a more appropriate luminescent label remains a challenging task and has recently emerged as a focal point in the chemistry and sensing communities. Upconversion (UC) nanophosphors, which are excited in the infrared region instead of the UV and visible region to emit in the visible domain, may be an alternative [16–18]. Compared to organic fluorophores and quantum dots, UC nanophosphors exhibit long fluorescence lifetimes, low photobleaching, high quantum yields, narrow emission peak, large Stokes shifts, and low toxicity. Furthermore, their low

* Correspondence to: Harbin Institute of Technology, 92 Xidazhi Street, Harbin 150001, China. Tel./Fax: +86 451 8641 8409.
** Corresponding author at: State Key Laboratory of Urban Water Resource and Environment, Harbin Institute of Technology, Harbin 150001, China.
E-mail addresses: wangzhijiang@hit.edu.cn (Z. Wang), jiangzhaohua@hit.edu.cn (Z. Jiang).
[1] These authors contributed equally to this work.

0039-9140/$ - see front matter © 2013 Elsevier B.V. All rights reserved.
http://dx.doi.org/10.1016/j.talanta.2013.02.069

autofluorescence background, high chemical stability, and tunable optical properties, which can be tuned by varying the lanthanide dopants and host matrix, make such nanophosphores suitable fluorescence labels. In particular, the luminescence from biological, toxicological and environmental samples (background) upon excitation with IR radiation is extremely low. All of these favorable properties demonstrate the great potential of UC nanocrystals in the analysis of biological, toxicological and environmental samples.

Here, based on LRET between $NaYF_4$:Yb,Ho nanocrystals and gold nanoparticles, we demonstrate a novel, highly sensitive and selective nanosensor for the detection of cartap. The nanosensor, a $NaYF_4$:Yb,Ho/Au nanocomposite, was synthesized through the self-absorption of gold nanoparticles on the surface of thiol-functionalized UC nanocrystals. The nanocomposites were then modified with mercaptopropionic acid (MPA) in which the hydrogen-bonding recognition between MPA and cartap via OH-N and NH_2-O pulls the nanocomposites closer, resulting in LRET taking place between $NaYF_4$:Yb,Ho nanocrystals (donors) and Au nanoparticles (acceptors) located on the other nanocomposites (Fig. 1). The aggregation status of $NaYF_4$:Yb,Ho/Au nanocomposites was determined by the decrease in the UC emission intensity, and thus, detection of cartap was achieved by examining the quenching of UC emission of the $NaYF_4$:Yb,Ho/Au nanocomposites.

2. Materials and methods

2.1. Reagents and chemicals

Yttrium oxide (Y_2O_3, 99.99%), ytterbium oxide (Yb_2O_3, 99.99%), holmium oxide (Ho_2O_3, 99.99%), hydrogen tetrachloroaurate trihydrate ($HAuCl_4 \cdot 3H_2O$, 99.99%), sodium borohydride ($NaBH_4$, 99%), 3-mercaptopropyltrimethoxysilane (MPTMS, 95%), and tetraethoxy silane (TEOS, 99%) from Aldrich were used as received. Deionized water with high resistivity (18.2 MΩ · cm) was obtained using a TKA GenPure ultrapure water system. All of the glassware was cleaned with aqua regia ($HCl:HNO_3 = 3:1$ vol%), rinsed with ultrapure water, and then dried in an oven prior to use. All reagents were of analytical grade and used as received, without further purification.

2.2. Characterization

Transmission electron microscopy (TEM) images of the samples were obtained on a Tecnai G2 F30 electron microscope under an accelerating voltage of 300 keV. X-ray diffraction (XRD) experiments were performed on a Rigaku D/max-γB diffractometer equipped with a rotating anode and a Cu Kα source operated at 40 kV and 100 mA. UV/visible (UV/vis) absorption spectra were collected using a calibrated spectrophotometer (Cary 4000, Varian) at room temperature. The room temperature UC luminescence spectra were obtained by a lens-coupled monochromator (Zolix Instruments Co. Ltd., Beijing) with 3-nm spectral resolution with an attached photomultiplier tube (Hamamatsu CR131) under excitation at 970 nm by a diode laser.

2.3. Synthesis of $NaYF_4$:Yb,Ho nanocrystals

Nanocrystals of $NaYF_4$ doped with 2 mol% Ho^{3+} and 20 mol% Yb^{3+} were prepared via a hydrothermal process. In brief, NaOH (25 mmol), water (5 mL), ethanol (5 mL) and oleic acid (15 mL) were mixed together. Then, 1.2 mmol of an aqueous solution of $Ho(NO_3)_3$, $Yb(NO_3)_3$ and $Y(NO_3)_3$ were introduced. Subsequently, aqueous NaF was added to the solution. After approximately 10 min, the solution

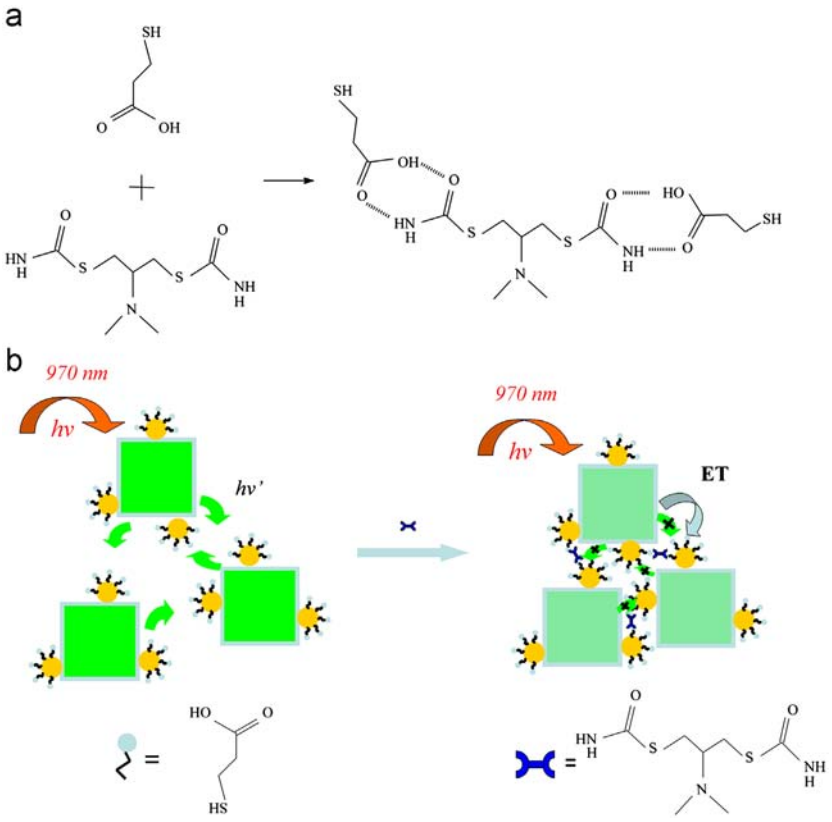

Fig. 1. Schematic illustration for the detection of cartap based on LRET. Hydrogen-bonding recognition between cartap and MPA (a), and detection of cartap using the LRET between $NaYF_4$:Yb,Ho and gold nanoparticles in adjacent nanocomposites (b). ET = energy transfer.

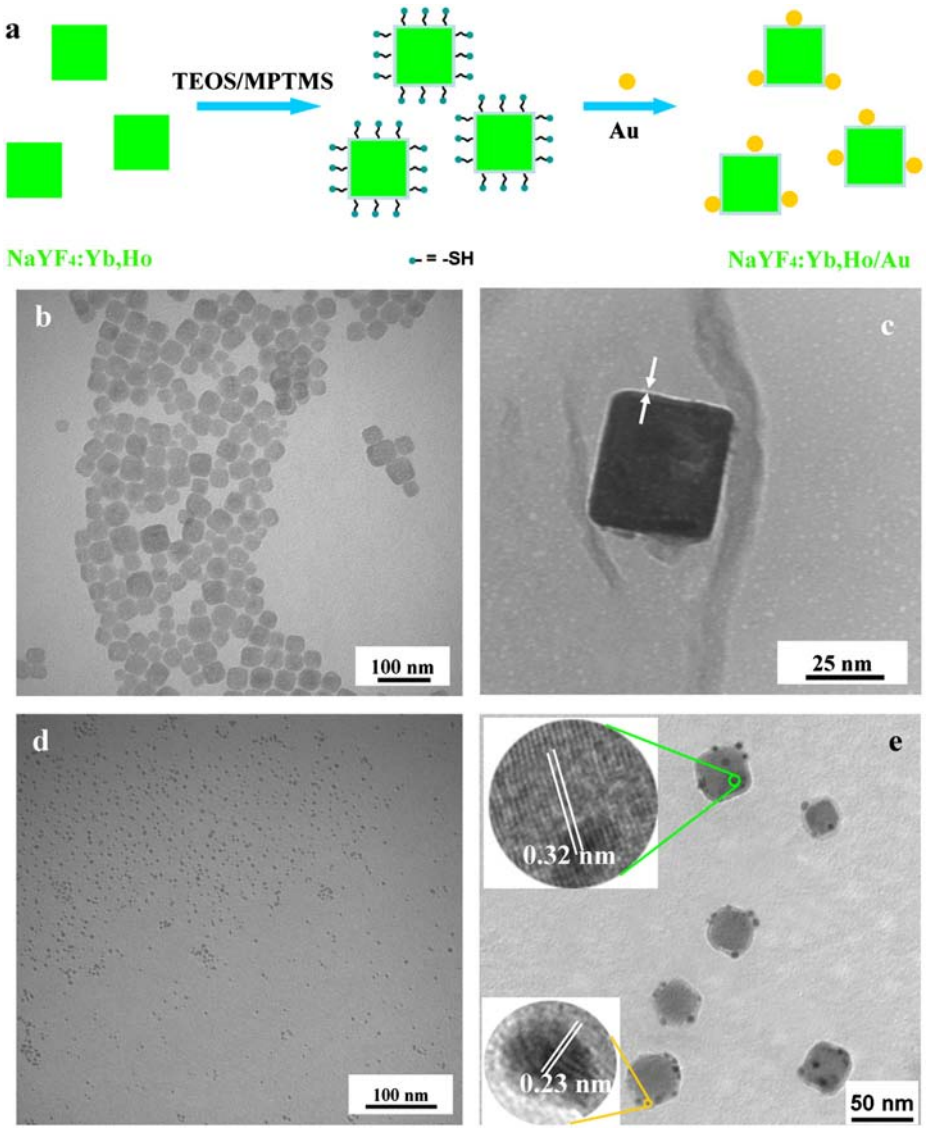

Fig. 2. Schematic illustration for the fabrication of $NaYF_4$:Yb,Ho/Au nanocomposites (a), TEM image of $NaYF_4$:Yb,Ho nanocrystals (b), mercapto-functionalized $NaYF_4$:Yb,Ho nanocrystals (c), Au nanoparticles (d), and $NaYF_4$:Yb,Ho/Au nanocomposites (e). The inset contains the HRTEM images.

was transferred to a 50 mL autoclave and hydrothermally treated at 180 °C for 18 h.

2.4. $NaYF_4$:Yb,Ho nanocrystals coated with a mercapto-silica shell

Typically, 125 mg of $NaYF_4$:Yb,Ho nanocrystals were dispersed in cyclohexane by sonication. Then, 1.25 mL of 25% ammonia and 50 μL of TEOS was added to this solution and stirred for 6 h. Finally, 70 μL of MPTMS was introduced to the solution and stirred for an additional 6 h.

2.5. Fabrication of $NaYF_4$:Yb,Ho/Au nanocomposites

$NaYF_4$:Yb,Ho/Au nanocomposites were synthesized using a layer-by-layer technology. First, gold nanoparticles were prepared as described previously [19]. The gold colloidal solution was subsequently dropped into the thiol-modified $NaYF_4$:Yb,Ho colloidal solution. After 15 min, the $NaYF_4$:Yb,Ho/Au nanocomposites were collected using an ultrasonic redispersion-centrifugation process. Then, the nanocomposite suspension was adjusted so that the Yb concentration was 2 nM. All of the suspensions of $NaYF_4$:Yb,Ho/Au in the present research maintained this concentration.

2.6. Analysis of spiked samples

To measure cartap in the farm produce and water samples, local Chinese cabbage, local grape juice, apples imported from the USA, prunes imported from France and local river water were obtained and treated according to previous reports [20,21]. Ten grams of local Chinese cabbage was weighed, finely chopped, dissolved in 50 mL methanol and then ultrasonicated for 60 min. The sample mixture was centrifuged, and the supernatant was filtered. The filtrate was further purified with activated carbon to remove impurities, such as pigments. The obtained sample solution was washed with 10 mL methanol and concentrated until almost dry at 50 °C by vacuum rotary evaporator. The residue was diluted with water to 5 mL.

For the grape, apple and prune juice samples, 10.0 mL of juice was extracted from the fresh fruits without any pre-separation or pre-concentration. After the samples were homogenized, they were centrifuged for 5 min at 3000 rpm. The supernatants were collected and then filtered with activated carbon. Finally, the obtained sample was diluted with water to 5 mL.

A water sample was collected from Songhua River in the city of Harbin without any pre-separation or pre-concentration. The

sample was centrifuged for 5 min at 3000 rpm, and the supernatant was collected.

Finally, these solutions were maintained at a pH value of 4.0. A certain amount of cartap was added to the samples. After the above procedure was completed, the spiked samples were mixed with the MPA-$NaYF_4$:Yb,Ho/Au-based nanosensor (pH=4.0) to perform the UC emission measurement. All of the samples were incubated for 10 min before the UC emission measurement was collected.

3. Results and discussion

Fig. 2a illustrates the strategy for the synthesis of UC nanocrystal-Au nanoparticle nanocomposites. The UC nanocrystals we chose to use were $NaYF_4$:Yb,Ho nanocrystals. As shown in Fig. 2b, the cubic $NaYF_4$:Yb,Ho nanocrystals have a size of approximately 40 nm. As during the hydrothermal reaction, the carboxyl groups of the oleic acid molecules interacted strongly with the rare-earth ions; the produced $NaYF_4$:Yb,Ho nanocrystals were protected by a layer of oleic acid with the chains outside of the particle, which allowed them to bond tightly with the gold nanoparticles. Because the gold nanoparticles have a robust interaction with thiol groups, the $NaYF_4$:Yb,Ho nanocrystals were processed using a modified Stöber method with a sol-gel modification [22]. The $NaYF_4$:Yb,Ho nanocrystals act as seeds for the deposition of the silica shell. The functional groups at the surface of these unmodified silica nanoparticles are predominantly silanol (Si-OH) or ethoxy (Si-OCH2CH3) groups. These groups were treated with the silane coupling agent MPTMS ([Si(OCH3)3–(CH2)3–SH]) to obtain thiol-functionalized $NaYF_4$:Yb,Ho@SiO2 colloids with a shell thickness of approximately 3 nm (shown in Fig. 2c). Finally, the gold nanoparticle colloids were added to the $NaYF_4$:Yb,Ho nanocrystals and tightly linked with gold nanoparticles in which the mercapto-silica shell acted as the bridge layer, as shown in the TEM images in Fig. 2e. It can be seen from the HRTEM images that the lattice spacing between the two adjacent planes of the inner materials was 0.32 nm, which corresponds to the distance between two (111) planes in a face-centered cubic (fcc) $NaYF_4$ crystal. The outer nanoparticles, which had a higher contrast compared to the inner cubic nanocrystals, had a lattice spacing of 0.23 nm corresponding to the (111) plane of fcc Au.

The optical properties of the fabricated $NaYF_4$:Yb,Ho/Au nanocomposites were studied by the examination of their UC luminescence and UV-vis absorption spectra. The nanocomposite produces UC luminescence. Under excitation at 970 nm, two emission bands are observed in the UC spectrum of the $NaYF_4$:Yb,Ho/Au nanocomposites: a strong green emission at 541 nm and a weak red emission at 647 nm (shown in Fig. 3a), which stem from the 4f configuration transitions of Ho^{3+} from $^5S_2/^5F_4$ and $^5F_5$ to the ground state $^5I_8$, respectively. Unlike organic fluorescent dyes, which display broad emission spectra and small Stokes shifts, the UC nanocrystal-based nanocomposite exhibits a narrow emission spectrum and large Stokes shift. In addition, because the gold nanoparticles are loaded on the surface of the nanocomposites, an absorption band ranging from 440 to 800 nm with a peak at 534 nm is observed in the UV/vis absorption spectrum (Fig. 3b), which is attributed to the surface plasmon resonance of gold [23–25].

In the nanocomposites, the UC emission at 541 nm matches the extinction band, which results in the occurrence of LRET and a decrease in the UC emission intensity compared to the $NaYF_4$:Yb, Ho nanocrystals that are not linked with gold. Although the inner-particle LRET decreases the UC intensity, a colloidal suspension with $NaYF_4$:Yb,Ho/Au nanocomposites has stable optical properties. In the nanocomposite suspension containing a Yb concentration of 2 nM, the inter-particle LRET is negligible, as the distance

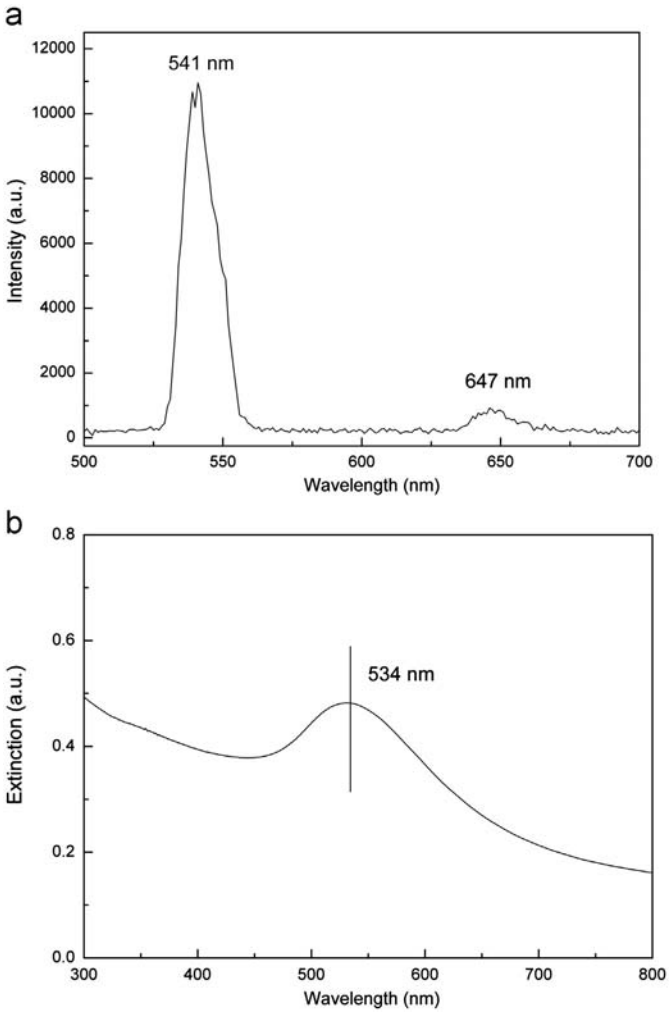

Fig. 3. UC emission (a) and UV/vis (b) spectra of the $NaYF_4$:Yb,Ho/Au nanocomposites.

between the nanocomposites in the colloidal solution far exceeds the Förster distance, which must be within 10 nm [11,26]. However, when molecules that can link the nanocomposites together and shorten their distance are added to the solution, inter-particle LRET takes place, and the UC emission of the nanocomposites is further decreased.

The $NaYF_4$:Yb,Ho/Au nanocomposites were utilized to detect cartap in solution. Initially, the $NaYF_4$:Yb,Ho/Au nanocomposites were modified with MPA by the ligand-exchange reaction. The MPA molecules were linked to the nanocomposites via Au-S bonds. This modification has little influence on the optical properties of the nanocomposites [19]. Upon exposure of the MPA-modified $NaYF_4$:Yb,Ho/Au nanocomposites to cartap, the aggregation of nanocomposites was driven by the binding to cartap molecules, as shown in Fig. 1, which resulted in a decrease in the UC emission. Fig. 4a displays the response of a suspension of $NaYF_4$:Yb,Ho/Au at a pH of 4.0 to cartap. With the addition of the cartap, the red color of the nanocomposite colloid changes to blue when the concentration of cartap is 300 ppb or the nanocomposites are precipitated in a high concentration of cartap (1000 ppb), as demonstrated in the inset of Fig. 4a. The cartap-stimulated aggregation of the MPA-$NaYF_4$:Yb,Ho/Au nanocomposites is further supported by the TEM image shown in Fig. 4b. Due to the strong binding of cartap with the carboxyl groups of MPA, irregular nanocomposite aggregates with diameters ranging from

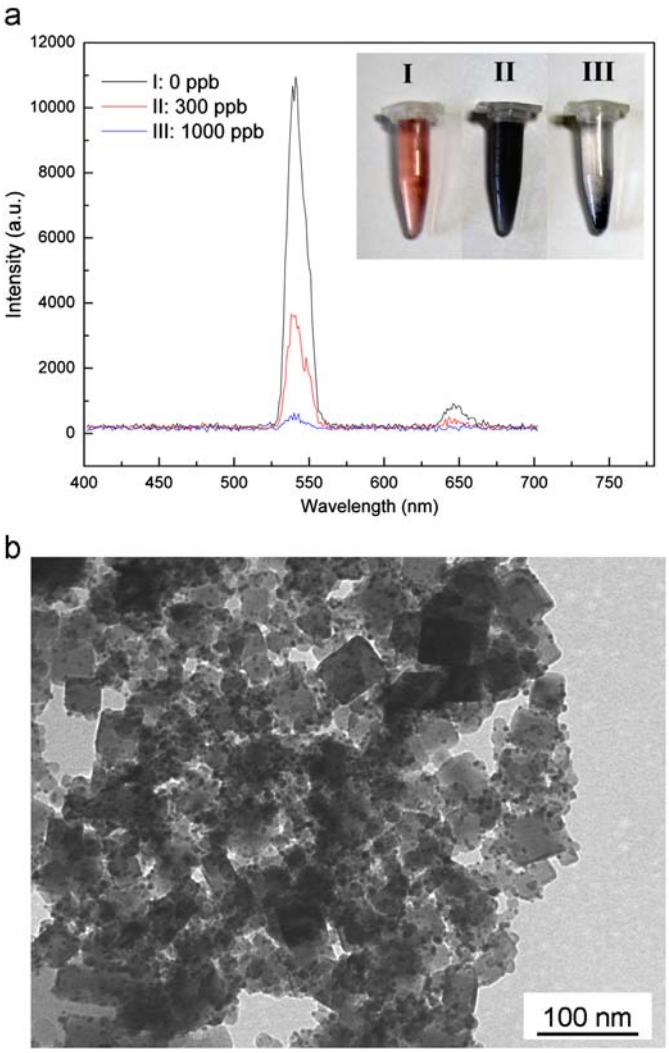

Fig. 4. UC emission spectra of MPA-$NaYF_4$:Yb,Ho/Au nanosensors with the addition of 0 ppb, 300 ppb and 1000 ppb of cartap; the inset contains photographic images of the nanosensors with different concentrations of cartap (a) and a TEM image of the solution containing MPA-$NaYF_4$:Yb,Ho/Au nanosensors with 1000 ppb of cartap (b).

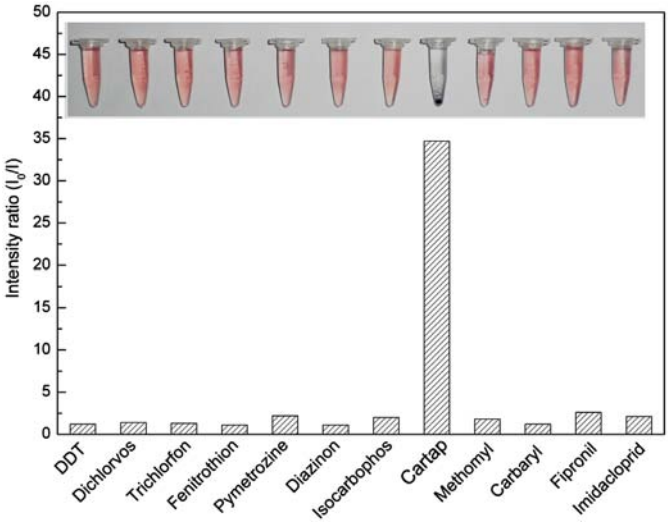

Fig. 5. UC emission ratio, I_0/I, of the MPA-$NaYF_4$:Yb,Ho/Au nanosensors with the addition of 1000 ppb pesticides. The inset contains the photographic image of the nanosensors with different pesticides, its order being same as the bottom order.

a few hundred nanometers to micrometers were observed. In this case, the distance between the $NaYF_4$:Yb,Ho nanocrystals and the Au nanoparticles located on the other nanocomposites is greatly decreased, which results in the occurrence of LRET and the decreased UC emission intensity with an increase in the cartap concentration.

The selectivity of the MPA-$NaYF_4$:Yb,Ho/Au-based nanosensors for cartap was evaluated in the presence of various pesticides. Fig. 5 displays the changes in the UC luminescence intensity of the nanocomposites upon interaction with DDT, dichlorvos, trichlorfon, fenitrothion, pymetrozine, diazinon, isocarbophos, methomyl, carbaryl, fipronil and imidacloprid, as well as cartap pesticides at a concentration of 1000 ppb. The MPA-$NaYF_4$:Yb,Ho/Au particle responds selectively toward cartap by approximately 20-fold relative to the other pesticides. The reason for the selective response of the MPA-$NaYF_4$:Yb,Ho/Au nanoparticles to cartap could be explained as follows. It is necessary for the analytes to have more than one amino group on the molecular structure to drag the nanocomposites closer. In addition, because the pK_a value of MPA is 4.87, at a low pH, less carboxylic acid is ionized, which leads to more hydrogen bonding between MPA and cartap, including OH-N and NH_2-O, as depicted in Fig. 1. Because cartap has more linking groups than do the other tested molecules, the MPA-$NaYF_4$:Yb,Ho/Au nanocomposites are highly selective for cartap.

Quantitative analysis was performed after the addition of different concentrations of cartap in the solution of MPA-$NaYF_4$:Yb,Ho/Au nanoparticles. The intensity of the UC emission peaks decreased with an increase in the cartap concentration, as illustrated in Fig. 6. A linear regression (R^2=0.993) was found between the natural logarithm of the UC peak intensity at 541 nm and cartap concentration over the range of 10–1000 ppb (inset of Fig. 6). This linear plot provides a calibration for the quantitative detection of cartap. The detection sensitivity of the fabricated MPA-$NaYF_4$:Yb,Ho/Au-based nanosensors for cartap could reach as low as 10 ppb. The standard for the maximum allowable level of cartap in the most farm produce is limited to approximately 1 ppm, according to the policies of the Environmental Protection Agencies (EPAs) of the United States and China [27,28]. The current experiment indicates that our nanocomposite probe is capable of measuring the cartap concentration, even at the 10 ppb level, which is approximately two orders of magnitude higher than the EPA standard.

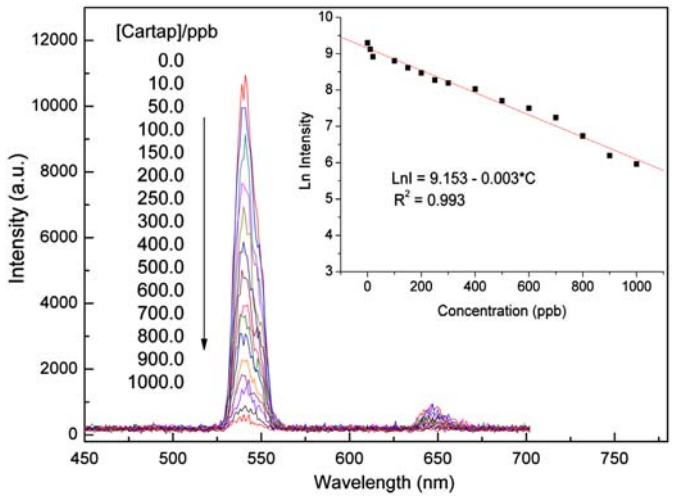

Fig. 6. LRET based detection of cartap. UC emission spectra of $NaYF_4$:Yb,Ho/Au nanocomposites with different concentrations of cartap. The inset shows the linear relationship between the natural logarithm of the UC peak intensity (ln I) at 541 nm and the cartap concentration over the range of 0–1000 ppb.

Table 1
Detection of trace cartap in samples via the proposed method and GB/T 20769-2008[a].

	Actual concentration[b]	The proposed method		GB/T 20769-2008	
		Detected concentration (mean, $n=6$)	Recovery (%)	Detected concentration (mean, $n=6$)	Recovery (%)
Chinese cabbage	100	101.1 ± 1.2	101.1 ± 1.2	104.1 ± 1.0	104.1 ± 1.0
Chinese cabbage	300	309.9 ± 2.7	103.3 ± 0.9	291.9 ± 4.8	97.3 ± 1.6
Local grape juice	100	99.7 ± 1.1	99.7 ± 1.1	98.2 ± 0.9	98.2 ± 0.9
Local grape juice	300	297.3 ± 1.8	99.1 ± 0.6	305.4 ± 4.2	101.8 ± 1.4
USA apple juice	100	98.7 ± 0.8	98.7 ± 0.8	101.7 ± 1.5	101.7 ± 1.5
USA apple juice	300	305.4 ± 1.9	101.8 ± 0.6	308.5 ± 3.9	102.8 ± 1.3
French prune juice	100	100.7 ± 1.3	100.7 ± 1.3	99.2 ± 0.9	99.2 ± 1.9
French prune juice	300	298.5 ± 2.1	99.5 ± 0.7	306.5 ± 3.8	102.3 ± 1.3
Songhua river water	100	97.8 ± 0.7	97.8 ± 0.7	102.8 ± 1.1	102.8 ± 1.1
Songhua river water	300	294.6 ± 2.4	98.2 ± 0.8	297.6 ± 2.4	99.2 ± 0.8

[a] n is the number of repeats.
[b] The concentration unit is ppb.

The applicability and validation of this novel MPA-$NaYF_4$:Yb,Ho/Au-based nanosensor for the analysis of cartap in grape, apple, prune, Chinese cabbage and river water was investigated, and the results were compared to the results obtained from the LC-MS-based method of the Chinese National Standards GB/T 20769-2008. The results demonstrate that there is no cartap detected in the five sample types. However, we chose the samples to evaluate the potential application of the MPA-$NaYF_4$:Yb,Ho/Au-based nanosensor because the chosen five sample types have some coexisting interference, including inorganic salts and even trace amounts of other small organic molecules, as shown in Table S2. Therefore, the juice, Chinese cabbage and river water samples, which were found to be free from cartap, were spiked with different concentrations of cartap, pretreated and analyzed according to the procedures described in Experimental Section. At the same time, the cartap in the treated samples was detected following the method of GB/T 20769-2008. For each sample, six parallel experiments were carried out. As presented in Table 1, the detected cartap concentration in the polluted samples from the two methods is in good agreement. A slight difference might be ascribed to the different conditions and assay procedures. Although there were salt ions, such as Na^+, K^+, Ca^{2+}, Mg^{2+}, Zn^{2+}, as well as organic molecules, including vitamins and organic acids, present in the sample matrices, the recoveries of these measurements by the MPA-$NaYF_4$:Yb,Ho/Au-based nanosensor were excellent and varied from 96.5% to 104.2%. In addition, the proposed MPA-$NaYF_4$:Yb,Ho/Au-based nanosensor for cartap is far easier to use than the LC-MS-based method. These results indicate that the developed MPA-$NaYF_4$:Yb,Ho/Au-based nanosensor has great potential applications for detecting environmentally relevant concentrations of cartap.

As is well known, the reliable performance requires consistent properties. The MPA-$NaYF_4$:Yb,Ho/Au nanocomposites can be stored for weeks when the pH is adjusted to 7.0. Stored at 4 °C, the nanocomposite-based nanosensor is stable, and no apparent luminescence loss can be observed within 90 days relative to measurements performed on freshly prepared nanocomposites (Fig. S1).

4. Conclusions

The present study has introduced a novel UC nanocrystal/Au nanoparticle nanocomposite-based LRET nanosensor for screening cartap. The as-prepared nanosensor combines the merits of both gold and UC nanocrystals and is formed by chemical bond linkage. The stable UC luminescence and easy functionalization of gold allow the nanocomposites to sense the presence of cartap based on UC luminescence quenching through cartap-induced aggregation. Under the optimal conditions, the sensitivity of the nanocomposites for cartap is 10 ppb, which is two orders of magnitude higher than the EPA standard limit. This nanosensor can detect cartap in farm produce with satisfactory results. The proposed chemosensor based on LRET exhibits good sensitivity, selectivity and accuracy, providing a simple and rapid method for the detection of cartap.

Acknowledgments

The authors appreciate the financial support of the National Natural Science Foundation of China (Nos. 51102067, 81101087, 81130028 and 31210103913), Science and Technology Research Project of Heilongjiang Education Department (No. 12511325), China Postdoctoral Science Foundation (20110491052, 2012T50321, 2012M510992), Heilongjiang Postdoctoral Foundation (LBH-Z10139, LBH-Z11054), Medical Scientific Research Foundation of Heilongjiang Province Health Department (2011-165) and the Fundamental Research Funds for the Central Universities (Grant no. HIT NSRIF. 2010067).

Appendix A. Supporting information compact-standard

Supplementary data associated with this article can be found in the online version at http://dx.doi.org/10.1016/j.talanta.2013.02.069.

References

[1] Z. Komala Bull, Environ. Contam. Toxicol 28 (1982) 660–663.
[2] Y. Kim, J. Jung, S. Oh, K. Choi, J. Environ. Sci. Health B 43 (2008) 56–64.
[3] S. Zhou, Q. Dong, S. Li, J. Guo, X. Wang, G. Zhu, Aqua. Toxicol 95 (2009) 339–346.
[4] H.K. Boorugu, A. ChrispalJ Indian, Crit. Care Med. 16 (2012) 58–59.
[5] E. Kurisaki, N. Kato, T. Ishida, A. Matsumoto, K. Shinohara, K. Hiraiwa, Clin. Toxicol. 48 (2010) 153–155.
[6] B. Kanrar, S. Mandal, A. Bhattacharyya, J. AOAC Int. 93 (2010) 411–424.
[7] I. Ferrer, E.M. Thurman, J. Chromatogr. A 1175 (2007) 24–37.
[8] C.C. Huang, Z. Yang, K.H. Lee, H.T. Chang, Angew. Chem. Int. Ed. 46 (2007) 6824–6828.
[9] J.H. Li, Z. Zhang, S.F. Xu, L.X. Chen, N. Zhou, H. Xiong, H.L. Peng, J. Mater. Chem. 21 (2011) 19267–19274.
[10] E. Mohabbati-Kalejahi, V. Azimirad, M. Bahrami, A. Ganbari, Talanta 97 (2012) 1–8.
[11] K.E. Sapsford, L. Berti, I.L. Medintz, Angew. Chem. Int. Ed. 45 (2006) 4562–4589.
[12] A.R. Clapp, I.L. Medintz, H. Mattoussi, Chem. Phys. Chem 7 (2006) 47–57.
[13] Y. Zhao, Y. Ma, H. Li, L. Wang, Anal. Chem. 84 (2012) 386–395.
[14] H. Azab, A. Duerkop, E. Mogahed, F. Awad, R. Abd El Aal, R. Kamel, J. Fluoresc. 22 (2012) 659–676.
[15] X. Wu, Z. Wu, Y. Yang, S. Han, Chem. Commun. 48 (2012) 1895–1897.

[16] F. Wang, Y. Han, C.S. Lim, Y.H. Lu, J. Wang, J. Xu, H.Y. Chen, C. Zhang, M.H. Hong, X.G. Liu, Nature 463 (2010) 1061–1065.
[17] L.Y. Wang, Y.D. Li, Chem. Mater. 19 (2007) 727–734.
[18] F. Wang, X.G. Liu, Chem. Soc. Rev. 38 (2009) 976–989.
[19] Z.J. Wang, L.N. Wu, H.J. Liang, W. Cai, Z.G. Zhang, Z.H. Jiang, J. Alloy Compd 509 (2011) 9144–9149.
[20] H. Mercan, E. Yilmaz, R. Inam, J. Hazard. Mater. 141 (2007) 700–706.
[21] H. Li, J. Guo, H. Ping, L. Liu, M. Zhang, F. Guan, C. Sun, Q. Zhang, Talanta 87 (2011) 93–99.
[22] W. Stöber, A. Fink, E. Bohn, J. Colloid Interf. Sci 26 (1968) 62–69.
[23] Z.J. Wang, L.N. Wu, W. Cai, Chem. Eur. J 16 (2010) 1459–1463.
[24] Z.J. Wang, L.N. Wu, W. Cai, Z.H. Jiang, J. Mater. Chem. 22 (2012) 3632–3636.
[25] S. Link, M.A. El-Sayed, J. Phys. Chem. B 103 (1999) 4212–4217.
[26] J. Zhang, Y. Fu, M.H. Chowdhury, J.R. Lakowicz, J. Phys. Chem. C 111 (2007) 11784–11792.
[27] FAO/WHO. Food Standards Program, 2nd Ed. Codex Alimentarius Commission, vol. 1, 1996.
[28] P. Caboni, G. Sarais, A. Angioni, V.L. Garau, P. Cabras, J. Agr. Food Chem. 53 (2005) 8644–8649.